ACS APPLIED MATERIALS & INTERFACES

Research Article

www.acsami.org

Investigation on New $CuInS_2$/Carbon Composite Counter Electrodes for CdS/CdSe Cosensitized Solar Cells

Xiaolu Zhang, Xiaoming Huang, Yueyong Yang, Shen Wang, Yun Gong, Yanhong Luo, Dongmei Li,* and Qingbo Meng*

Key Laboratory for Renewable Energy (CAS), Beijing Key Laboratory for New Energy Materials and Devices, Institute of Physics, Chinese Academy of Sciences, Beijing, 100190, People's Republic of China

Supporting Information

ABSTRACT: The search for semiconductor-sensitized solar cell (SSC) counter electrode alternatives has been a continuous effort and long ongoing work, while the studies in counter electrode kinetic performance and stability are important to improve the overall efficiency. Here, a ternary chalcopyrite compound $CuInS_2$ is first employed as counter electrode (CE) material for CdS/CdSe cosensitized solar cells. Besides, in order to increase the electron transfer activity at the counter electrode/electrolyte interface and stability, an appropriate amount of active carbon/carbon black mixture is introduced to afford $CuInS_2$/carbon composite electrodes. Electron transfer processes in $CuInS_2$-based electrodes are investigated in detail with the aid of electrochemical impedance spectroscopy and *I*–*E* measurement. Up to 4.32% of the light-to-electricity conversion efficiency has been achieved for the CdS/CdSe SSCs with the $CuInS_2$/carbon composite electrode. Besides, a preliminary long-term stability test reveals that the new $CuInS_2$/carbon composite counter electrode exhibits good stability after being kept in the dark at room temperature and without current flow for 1000 h.

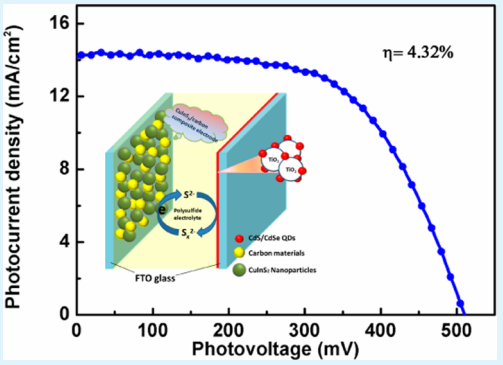

KEYWORDS: *semiconductor-sensitized solar cell, counter electrode, carbon, chalcopyrite, composite electrode*

1. INTRODUCTION

The key issue of the study in solar cells is to pursue higher energy conversion efficiency, lower cost, longer duration, and environmentally benign manufacture and operation. For this purpose, some new concepts, new materials, and new architecture have been introduced into the solar cells. Inorganic semiconductors as light absorbing materials exhibit some outstanding properties,[1] such as strong photoresponse, multiple exciton generation,[2] tunable band gaps,[3,4] easy fabrication, low cost, etc. Recently, inorganic semiconductors as the sensitizers for sensitized solar cells, so-called semiconductor-sensitized solar cells (SSCs), have received much research interest. Various inorganic semiconductor materials, such as CdS,[5,6] CdSe,[7,8] $CuInS_2$,[9] Sb_2S_3,[10] InP,[11] CdTe,[12] and PbS,[13] were applied in SSCs, and several milestones have been reached. For example, Meng et al. optimized the TiO_2 photoanodic structure for CdS/CdSe SSCs and PbS/CdS SSCs, which achieved 4.92% and 3.82% efficiency, respectively.[13,14] Kamat et al. reported the Mn-doped CdS/CdSe cosensitized solar cells with 5.4% efficiency.[15] Seok et al. fabricated the Sb_2S_3 sensitized TiO_2 heterojunction solar cell using conjugated polymers as hole-transporting materials, presenting 6.18% efficiency.[10] However, the cell performance of SSCs is still far satisfactory in comparison with the conventional dye-sensitized solar cells (DSCs), mainly because serious photogenerated electron recombination loss and inner energy loss occur at the electrolyte/electrode interfaces.[16−19]

As an important part of the sandwich-type solar cells, the counter electrode (CE) is responsible for catalyzing the reduction of the redox shuttle in the electrolyte by electrons from external circuit and keeping the cell running.[20] To SSCs, a polysulfide (S_x^{2-}/S^{2-}) electrolyte system is usually adopted, which exhibits strong selectivity toward CEs. Conventional Pt electrode in DSCs is not suitable for SSCs because its strong chemiadsorption with sulfide ions results in low conductivity and poor catalytic activity.[21] Therefore, seeking ideal non-Pt electrode materials is stringent for highly efficient SSCs.

Some non-Pt electrode materials have been applied in the SSCs. In the early 1970s, Hodes and Cahen investigated two non-Pt electrodes for the polysulfide electrolyte, Teflon-bonded high surface area carbon loaded with electrocatalysts Co and Ni. Their preliminary results revealed that Co exhibited good activity.[22] Chang et al. reported the CuS/CoS counter electrode for CdS/CdSe SSCs, which presented 4.1% efficiency.[23] Zaban et al. used the PbS electrode for polysulfide-based CdS/CdSe SSCs and achieved 3% efficiency.[24] In particular, in situ prepared Cu_2S electrode on brass sheet is the most widely adopted counter electrode so far; however, this in situ preparative method suffers from continuous corrosion, eventually leading to the mechanical instability of the electrode

Received: January 21, 2013
Accepted: June 4, 2013
Published: June 4, 2013

and sealing problem.[15,25] Meng et al. fabricated CdS SSCs based on the activated carbon/carbon black electrode with 1.47% efficiency.[26] Yu et al. adopted open mesoporous carbon nanofibers with tailored nanostructure into CdSe SSCs and achieved 4.81% efficiency.[27] Particularly, some metal sulfide/carbon composite electrodes (i.e., Cu_2S/graphene oxide, PbS/carbon black) have been developed, which can present higher cell performance than the single material.[15,21,28] Although these works demonstrated considerable enhancement in the cell performance of SSCs, it is still hard to evaluate the electrocatalytic activity of the counter electrodes due to various influencing factors to the cell performance. Besides, some issues including high overpotential for polysulfide reduction at the counter electrode, large internal resistance, and improved stability in some cases are still unsolved. Therefore, it is necessary to continuously research low cost counter electrodes with high catalytic activity and satisfactory stability.

Ternary chalcopyrite $CuInS_2$ with low toxicity is an attractive light absorbing material for quantum dot solar cells.[9,29,30] In the meantime, $CuInS_2$ also exhibits good stability in the aqueous polysulfide electrolyte according to previous investigations.[31,32] However, no work has been reported to fabricate SSCs with $CuInS_2$ counter electrodes. In this respect, we first prepare the $CuInS_2$ counter electrode, which exhibits good catalytic activity toward the polysulfide electrolyte. Furthermore, by introducing an appropriate amount of active carbon/carbon black mixture into the $CuInS_2$ electrode to afford the $CuInS_2$/carbon composite electrodes, better conductivity and lower charge transfer resistance at the electrode/electrolyte interface has been achieved, thus leading to 4.32% conversion efficiency. Our investigation, on the variation of the efficiency of CdS/CdSe SSCs over 1000 h of preservation in the dark at room temperature, reveals that the $CuInS_2$/carbon composite electrodes in conjunction with 1 M polysulfide electrolyte is primarily stable.

2. EXPERIMENTAL SECTION

Materials. $CdCl_2{\cdot}2.5H_2O$, NH_4Cl, $CdSO_4{\cdot}8/3H_2O$, $Zn(CH_3COO)_2{\cdot}2H_2O$, $Na_2S{\cdot}9H_2O$, Na_2SO_3, thiourea, $Cu(CH_3COO)_2{\cdot}H_2O$, diethylene glycol (DEG), anhydrated $InCl_3{\cdot}4H_2O$, titanium(IV) isopropoxide, ammonia, and sulfur were from Sinopharm Chemical Reagent Co. Ltd. Sodium nitrilotriacetate (NTA) and selenium powder were purchased from Alfa Aesar Chemicals. Activated carbon was donated from Institute of Metal Research, Chinese Academy of Sciences. Carbon black (30−50 nm particle size) was from Degussa.[33] All the chemicals were directly used without further purification, and all the solutions for the electrolyte and semiconductor deposition were prepared by using Milli-Q high-purity water (Millipore Model RG). Na_2SeSO_3 was synthesized by heating selenium powder (26 mM) in an aqueous Na_2SO_3 solution (67 mM) at 70 °C for 3 h.[34] $CuInS_2$ NPs were prepared as follows: 3.0 g (15 mmol) of $Cu(CH_3COO)_2{\cdot}H_2O$ and 4.4 g (15 mmol) of $InCl_3{\cdot}4H_2O$ were dissolved in 200 mL of diethylene glycol (DEG) and heated up to 180 °C, followed by adding 2.3 g (30 mmol) of thioacetamide in 60 mL of DEG drop by drop while stirring, and kept at the same temperature for 3 h.[35,36] After cooling down to room temperature, the $CuInS_2$ precipitate was filtered, washed with ethanol for three times, and finally dried at 60 °C in a vacuum oven overnight. The electrode substrate is fluorine-doped tin oxide conducting glass (FTO, Pilkington; thickness: 2.2 mm; sheet resistance 14 $\Omega{\cdot}square^{-1}$). Before use, FTO glass was first washed with mild detergent, rinsed with distilled water for several times and subsequently with ethanol in an ultrasonic bath, and finally dried under air stream.

Preparation of $CuInS_2$-Based Counter Electrodes. The $CuInS_2$ paste was prepared typically as follows: 0.2 g of ethyl cellulose was first dissolved in 10 mL of terpineol by heating at 40 °C. Then, 2 g of the as-prepared $CuInS_2$ NPs, 1.2 mL of titanium(IV) isopropoxide, and the above ethyl cellulose/terpineol solution were ball-milled in the agate jar at 450 r/min for 12 h. The $CuInS_2$/carbon paste was prepared in the same way except for adding carbon black and activated carbon (1:1) mixture into the $CuInS_2$ paste in the appropriate weight ratio. The $CuInS_2$ or $CuInS_2$/carbon films were deposited on FTO-glass substrates by the doctor-blading technique. The films were then dried at 80 °C for 30 min and sintered in air at 400 °C for 30 min. For comparison, the carbon film containing carbon black and activated carbon (1:1) mixture was also prepared.

Fabrication of CdS/CdSe SSCs. A double layer TiO_2 photoanode was prepared on the FTO substrate by a doctor blading technique, which consisted of a 7 μm-thickness transparent layer with 20 nm anatase TiO_2 particles and a 3 μm-thickness light-scattering layer with 300 nm rutile TiO_2 particles and 20 nm anataseTiO_2 particles.[37] CdS/CdSe-sensitized photoanode was fabricated by a chemical bath deposition (CBD) technique.[14] Briefly, CdS nanoparticles were deposited onto TiO_2 nanoporous film in the aqueous solution of 20 mM $CdCl_2$, 66 mM NH_4Cl, 140 mM thiourea, and 230 mM ammonia for 50 min at 10 °C. Subsequently, CdSe nanoparticles were deposited on the CdS/TiO_2 film by immersing into the mixture solution of 80 mM Na_2SeSO_3, 80 mM $CdSO_4$, and 160 mM NTA. The CdS/CdSe decorated photoanode was finally passivated with ZnS by alternatively dipping the film into 0.1 M $Zn(CH_3COO)_2$ and 0.1 M Na_2S solutions for 1 min twice.[8] The CdS/CdSe-decorated TiO_2 film, polysulfide electrolyte (1 M Na_2S and 1 M S), and $CuInS_2$-based counter electrode were assembled into a sandwich-type cell.

Assembly of Symmetric Thin Layer Cells for Electrochemical Impedance Spectroscopy. The two identical electrodes ($CuInS_2$, $CuInS_2$/carbon and carbon) and the electrolyte inside was thermally sealed with a 25 μm-thickness hot-melt EVA (ethylene−vinyl acetate copolymer) gasket to give a sandwich-type cell. The polysulfide electrolyte was injected through the holes from the counter electrode side, and finally, the holes were sealed with EVA film and cover glass by heating.[25] An active area of thin layer symmetric cell is 0.50 cm^2.

Characterization. The surface morphologies were obtained using a scanning electron microscope (SEM, FEIXL30S-FEG). The X-ray diffraction (XRD, M18X-AHF, MAC Science) pattern was recorded with Cu Kα radiation source. $I-E$ measurement was performed by using a three-electrode system on ZAHNER IM6e electrochemical workstation with a scanning rate of 5 $mV{\cdot}s^{-1}$ in the potential range of −0.6 to 0.6 V at 20 °C. In the three-electrode system, our self-made electrode ($CuInS_2$-based or carbon electrodes) is the working electrode, a Pt electrode (area: 0.18 cm^2) is the counter electrode, and a Pt wire is the pseudo-reference electrode whose potential is that of the polysulfide electrolyte, respectively; the electrolyte is 1 M polysulfide solution. The adsorption/desorption data of $CuInS_2$/carbon film were analyzed using the BJH (Barrett, Joyner and Hanlenda) method for incremental pore volume distribution on an ASAP 2020 apparatus, Micromeritics. The resistivity of the $CuInS_2$/carbon (weight ratio 1:1) film was obtained at room temperature (300 K) by using a four-dot method on an Ecopia HMS-3000 Hall Effect Measurement System. A 10 μm-thickness $CuInS_2$/carbon film with the area of 1 cm × 1 cm for the resistivity measurement was obtained from depositing the paste on the nonconductive glass slide by a doctor-blading technique.

Measurement of Photocurrent Density−Photovoltage Curves ($J-V$) and Electrochemical Impedance Spectroscopy (EIS). The cells were irradiated by an Oriel solar simulator 91192 under AM 1.5 illumination (100 $mW{\cdot}cm^{-2}$), and the $J-V$ characteristics of the cells were recorded on Princeton Applied Research, Model 263A. For $J-V$ characteristics, a mask with a window of 0.15 cm^2 was clipped on the TiO_2 side to define the active area of the cell. The incident photon-to-current conversion efficiency (IPCE) was measured by using our homemade IPCE setup illuminated under 0.3−0.9 $mW{\cdot}cm^{-2}$ monochromic light.[38,39] Electrochemical impedance spectra (EIS) of symmetric thin layer cells were carried out on a ZAHNER IM6e electrochemical workstation in the frequency ranging from 0.1 to 10^5 Hz with a perturbation amplitude of 10 mV with zero bias

dx.doi.org/10.1021/am400268j | ACS Appl. Mater. Interfaces 2013, 5, 5954−5960

potential. The obtained impedance spectra were fitted with *Zview* software in terms of appropriate equivalent circuit.

Preliminary Study on the Stability of the $CuInS_2$-Based Counter Electrodes. For the stability test, a sealed SSC configuration was adopted, with a detailed fabrication procedure according to the literature.[14] Briefly, the CdS/CdSe-decorated photoanode and the $CuInS_2$/carbon electrode (or carbon electrode) were sealed by using the same method as the symmetric thin layer cell. The preliminary stability test was carried out as follows: the sealed small-size CdS/CdSe SSCs were kept in the dark at room temperature without any bias voltage or current flow, in which $J-V$ characteristics were measured every 2 or 3 days during 1000 h.[27]

3. RESULTS AND DISCUSSION

Figure 1 shows the XRD patterns of the $CuInS_2$ film, which can be identified well in comparison with the standard JCPDS-65-1572 patterns of tetragonal $CuInS_2$ whereas no obvious characteristic peaks of impurity phases such as copper sulfide (Cu_2S, JCPDS-46−1195) and indium sulfide are observed, indicating a basically satisfactory purity of the $CuInS_2$ film.[40] In the meantime, in order to find the influence of the polysulfide electrolyte on the composition of the $CuInS_2$ film, the XRD patterns of $CuInS_2$ film immersed into the polysulfide electrolyte for 4 weeks is also given. Comparison between the two patterns clearly displays that the diffraction peaks do not change before and after the polysulfide electrolyte treatment, indicating that the $CuInS_2$ film is basically stable in the electrolyte.

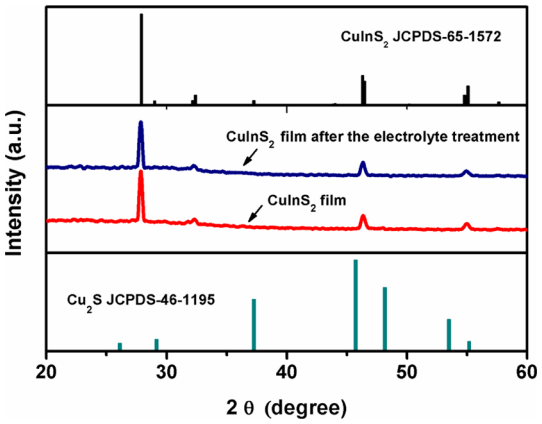

Figure 1. XRD patterns of the $CuInS_2$ films on FTO: $CuInS_2$ film treated with the polysulfide electrolyte (blue), untreated $CuInS_2$ film (red), and two standard cards $CuInS_2$ JCPDS-65-1572 (upper) and Cu_2S JCPDS-46-1195 (bottom).

Figure 2a shows the SEM image of as-prepared $CuInS_2$ NPs, which are used to prepare the $CuInS_2$-based pastes for the counter electrodes. We can see that the $CuInS_2$ NPs are basically spherical with the sizes in the range of 50−90 nm, but slight aggregation can also be observed. When forming the $CuInS_2$ film, the $CuInS_2$ NPs are connected together to afford the compact film after being sintered at 400 °C, as seen in Figure 2b. This morphology is supposed to be disadvantageous to the filtration of the electrolyte when it acts as the counter electrode for the SSCs. However, when an appropriate amount of active carbon/carbon black mixture is introduced into the $CuInS_2$ film, this situation clearly improves. As shown in Figure 2c, the $CuInS_2$ NPs uniformly disperse over the film, and no obvious aggregated particles are observed. Besides, some homogeneous nanopores are clearly seen, which are beneficial

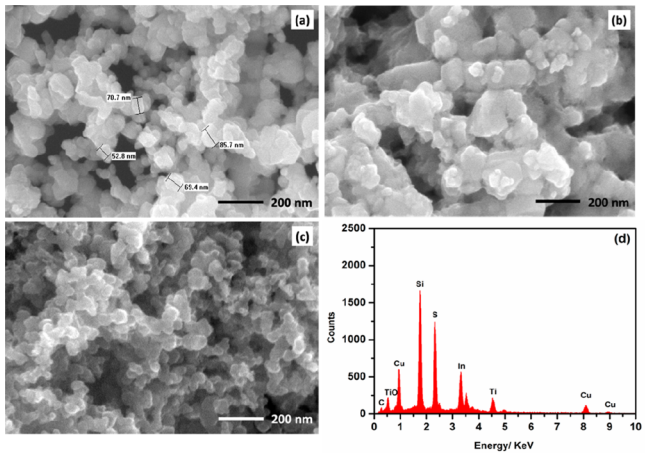

Figure 2. Representative SEM images of (a) as-prepared $CuInS_2$ particles, (b) the $CuInS_2$ film, (c) $CuInS_2$/carbon composite film with 1:1 weight ratio of $CuInS_2$ and carbon materials, and (d) EDX analysis of $CuInS_2$ film.

to the interfacial contact between the electrolyte and the electrode, thus leading to the improvement of the catalytic activity of the electrode.

Furthermore, EDX analysis is employed to semiquantitatively test the chemical composition of the $CuInS_2$ film on FTO glass, as shown in Figure 2d. According to the EDX data, the molar ratio of copper, indium, and sulfur is 1:0.86:1.79 in the $CuInS_2$ film, in which Cu element is slightly deviated from the standard chemical stoichiometry. It is supposed that there is slight Cu_2S impurity in the $CuInS_2$ film, which does not appear in the XRD.[40]

The textual structure of $CuInS_2$/carbon composite film was also investigated by N_2 adsorption/desorption. As shown in the inserted adsorption/desorption isotherm of Figure 3, the $CuInS_2$/carbon composite film presents type IV isotherms, and the hysteresis loop in the relative presure range between 0.5 and 0.8 suggests its mesoporous structure. The high-pressure part of the hysteresis loop ($0.9 < P/P_0 < 1.0$) is probably associated with textual larger pores that can be formed between $CuInS_2$ NPs.[41] Besides, the $CuInS_2$/carbon composite film has a wide pore-size distribution with the average pore size of 47.3 nm, as seen in Figure 3.

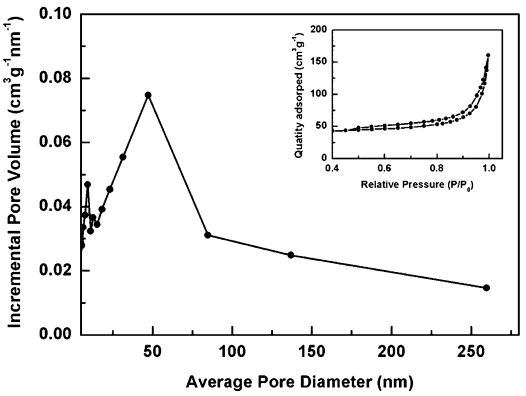

Figure 3. BJH desorption pore size distribution curves of $CuInS_2$/carbon composite film. Inset: the N_2 adsorption−desorption isotherm linear plot.

dx.doi.org/10.1021/am400268j | ACS Appl. Mater. Interfaces 2013, 5, 5954−5960

To further assess the catalytic activity of the $CuInS_2$-based electrodes, the $I-E$ measurement are given, which describe the relationship between the exchange current density and the potential; see Figure 4a. For comparison, the $I-E$ plot of carbon electrode is also presented. The measurement is based on a three-electrode system with $CuInS_2$-based (or carbon) electrode as the working electrode, a Pt sheet as the counter electrode, and a Pt wire as the pseudo-reference electrode whose potential is that of the polysulfide electrolyte. We can see that the $CuInS_2$/carbon electrode can exhibit higher exchange current density (J_0) toward the polysulfide ion reduction comparable to the single $CuInS_2$ and carbon electrodes.[42−45] This can be well explained that the existence of the homogeneous nanopores in the $CuInS_2$/carbon electrode and higher specific surface area of active carbon are beneficial to the filtration of the electrolyte into the electrode, well in agreement with the SEM images.[33,35] At the same time, good conductivity of carbon black also improves the electron transfer process in CEs, thus leading to the improvement on the catalytic activity. However, the catalytic activity of $CuInS_2$/carbon (1:1) composite electrode is still lower than that of Cu_2S/carbon in the same weight ratio, as shown in Figure S1, Supporting Information. By the aid of the four-dot method, the resistivity of the $CuInS_2$/carbon film (weight ratio 1:1) is 1.05 Ω·cm at room temperature (300 K), indicating that this $CuInS_2$/carbon film basically exhibits good electrical property.

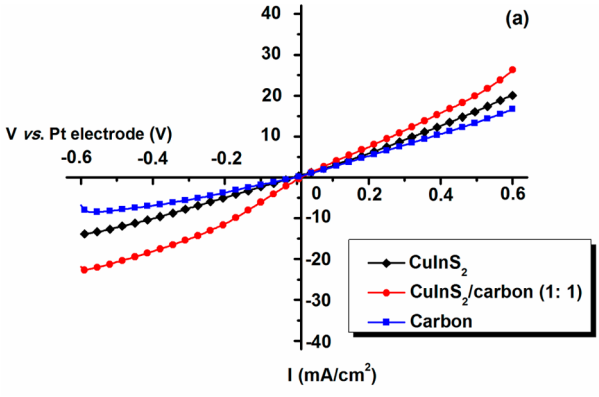

Figure 4. (a) $I-E$ curves of the $CuInS_2$ electrode, the $CuInS_2$/carbon (1:1) composite electrode, and the carbon electrode in a three-electrode testing system containing a Pt sheet counter electrode (area: 0.18 cm^2), a Pt wire as pseudoreference electrode whose potential is that of the polysulfide electrolyte, and the $CuInS_2$-based electrode (or carbon electrode) as the working electrode; (b) Variation of $I-E$ curves with the conservation time for the $CuInS_2$/carbon (1:1) composite electrode based on sealed symmetric thin-layer cells.

In order to investigate the influence of polysulfide electrolyte on catalytic activity of the $CuInS_2$/carbon electrode, a sealed symmetric thin layer cell was fabricated, which was kept in the dark for 20 days, and $I-E$ curves were obtained every 3−7 days. From Figure 4b, it is clearly observed that the catalytic activity of the $CuInS_2$/carbon electrode almost stays constant for 20 days, demonstrating its satisfactory stability. Besides, this $CuInS_2$/carbon electrode exhibits better stability than the Cu_2S/carbon (1:1) composite electrode although its catalytic activity is relatively lower than the Cu_2S/carbon composite electrode (Figure S2, Supporting Information).

When the CdS/CdSe-coated TiO_2 photoanode was incorporated with 1 M polysulfide electrolyte and the $CuInS_2$-based counter electrode to give a sandwich-type cell, the influence of various counter electrodes on the photovoltaic performance can be clearly distinguished; see Figure 5. Detailed cell parameters are presented in Table 1. For comparison, the cell performance of CdS/CdSe SSCs with in situ prepared Cu_2S counter electrode on brass and carbon electrode are also given.

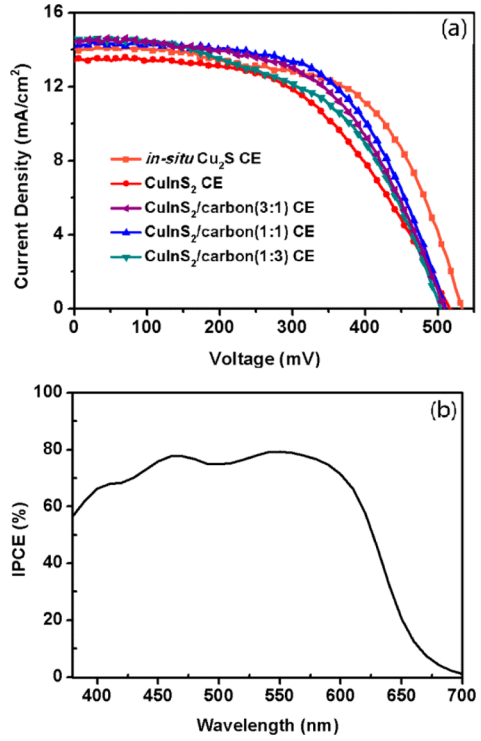

Figure 5. (a) Photocurrent density−photovoltage curves ($J-V$) for SSCs with various counter electrodes (in situ prepared Cu_2S electrode on brass, pure $CuInS_2$ electrode, three $CuInS_2$/carbon electrodes with different weight ratios); (b) IPCE spectra of the CdS/CdSe SSCs with $CuInS_2$/carbon electrode in 1:1 weight ratio of $CuInS_2$ and carbon.

As seen in Figure 5, the $CuInS_2$-based SSCs exhibit 3.63% of efficiency (η) under AM 1.5 illumination with 100 mW·cm^{-2}, which short-circuit photocurrent (J_{sc}), open-circuit photovoltage (V_{oc}), and fill factor (FF) are 13.43 mA·cm^{-2}, 518 mV, and 0.52, respectively. This result is comparable to our previous work about screen-printed Cu_2S/conductive carbon composite electrode with 3.71% of efficiency (η).[36] However, it is still lower than the SSCs with in situ prepared Cu_2S electrode, in which J_{sc}, V_{oc}, and FF are 13.92 mA·cm^{-2}, 531 mV,

dx.doi.org/10.1021/am400268j | ACS Appl. Mater. Interfaces 2013, 5, 5954−5960

Table 1. Photovoltaic Parameters for SSCs Based on Various Counter Electrodes under AM 1.5 Illumination of 100 mW·cm^{-2} and EIS Fitting Data for Symmetric Thin Layer Cells

counter electrodes[a]	J_{sc} (mA·cm^{-2})	V_{oc} (mV)	FF	η (%)	R_s (Ω)	R_{ct} (Ω·cm^2)
pure $CuInS_2$	13.43	518	0.52	3.63	12.58	75.45
$CuInS_2$:C = 3:1[b]	14.64	505	0.53	3.88	12.41	58.75
$CuInS_2$:C = 1:1[b]	14.16	512	0.60	4.32	10.96	18.79
$CuInS_2$:C = 1:3[b]	14.45	512	0.56	4.12	11.44	43.05
carbon	11.04	471	0.38	1.96	11.10	252.4

[a]The thickness of the electrode films is 10 μm. [b]Weight ratio.

and 0.61, respectively, yielding 4.51% of η, and this difference is largely attributed to the lower FF for $CuInS_2$-based SSCs. Therefore, for the $CuInS_2$ electrode, how to further improve the FF is the key to achieve highly efficient CdS/CdSe SSCs.

Considering the high specific surface area of active carbon and favorable conductivity of carbon black, the $CuInS_2$/active carbon/carbon black composite electrodes are further developed and applied in CdS/CdSe SSCs. We can see, from Figure 5 and Table 1, the SSCs with $CuInS_2$/carbon counter electrodes can exhibit the improved photocurrent densities (J_{sc}) and fill factors (FF). Among three $CuInS_2$/carbon counter electrodes with different carbon contents, the SSCs with the 1:1 weight ratio of $CuInS_2$ and carbon materials can exhibit the highest efficiency, in which J_{sc}, V_{oc}, and FF are 14.16 mA·cm^{-2}, 512 mV, and 0.60, respectively, yielding 4.32% of η. Especially, higher FF is mainly attributed to the improvement of the cell performance. As we know, several metal sulfides, including $CuInS_2$, can exhibit higher catalytic activity toward polysulfide electrolyte than carbon materials, while on the other hand, carbon materials are superior to Pt electrodes toward polysulfide electrolyte because of its good corrosion inertness toward polysulfide redox couple and larger specific surface area with porous structure, which accelerates the electron transfer and the electrolyte infiltration.[15,25,31,32] Therefore, the trade-off between $CuInS_2$ NPs and carbon materials is balanced when the ratio is 1:1, which can exhibit the best cell performance at that point.

As we know, a larger internal resistance of the solar cell will significantly reduce its overall performance, especially the fill factor (FF). Here, in order to further understand the influence of different weight ratios of the $CuInS_2$ and carbon materials on the cell performance, electrochemical impedance spectroscopy (EIS) is adopted, mainly for investigating on the sheet resistance and the charge transfer resistance at the electrode interfaces of the symmetric thin layer cells.[46−48] Here, five electrodes including $CuInS_2$ electrode, carbon electrode, and $CuInS_2$/carbon composite electrodes with three different carbon contents are included.

Figure 6b gives typical Nyquist plots of the five cells. Experimental curves are represented by symbols while the solid lines are the fitted curves, which are obtained with *Zview* software by using the equivalent circuit given in Figure 6a. The fitted parameter values are illustrated in Table 1. In general, the ohmic series resistance (R_s) consisting of the FTO layer, the electrode, and the electrolyte is determined in the high frequency range (over 10^5 Hz) where the phase is zero. For the $CuInS_2$ electrode, the R_s value is 12.58 Ω, slightly larger

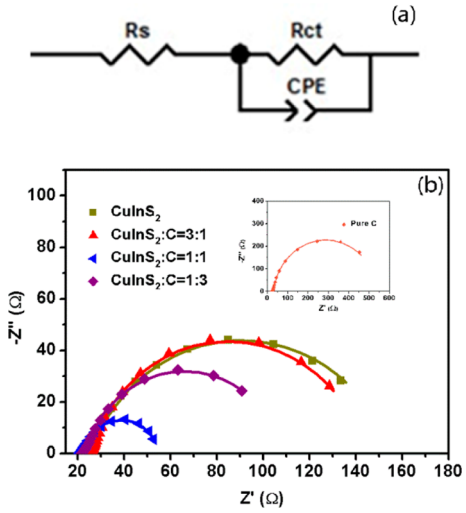

Figure 6. (a) Equivalent circuit for fitting the EIS; R_s: serial resistance; R_{ct}: change transfer resistance at the electrode/electrolyte interface; CPE: constant phase element of electrical double layer; (b) Nyquist plots of the symmetric thin layer cells with different electrodes (−■− $CuInS_2$, −▲− $CuInS_2$/carbon (3:1) electrode, −◀− $CuInS_2$/carbon (1:1) electrode, −♦− $CuInS_2$/carbon (1:3) electrode) measured at zero bias potential. The symbols and the solid lines are experimental and fitting curves, respectively. Inset: Nyquist plot of the symmetric thin layer cells with carbon electrode.

than those of $CuInS_2$/carbon composite electrodes, mainly due to the better conductivity of $CuInS_2$/carbon composite electrodes, indicating that the introduction of some carbon black into the $CuInS_2$ electrode will decrease the series resistances of the thin-layer cells. Besides, the R_s values of these $CuInS_2$/carbon composite counter electrodes are comparable to that of carbon electrode (11.10 Ω). In the middle frequency range of 10−10^5 Hz, the impedance associated with the heterogeneous electron transfer at the counter electrode/electrolyte interface can be established, including the charge transfer resistance (R_{ct}) and the double layer capacitance (CPE, constant phase element).[49,50] Several characteristics are summarized as follows: (1) the carbon electrode gives an unsatisfactory R_{ct} value (252.4 Ω·cm^2) comparable to the pure $CuInS_2$ electrode (75.45 Ω·cm^2); (2) the introduction of an appropriate amount of activated carbon and carbon black into the $CuInS_2$ electrode can improve the interfacial charge transfer property, and three electrodes with different carbon contents exhibit disciplinary R_{ct} values. Too much $CuInS_2$ NPs or carbon materials will bring about unsatisfactory R_{ct}. Instead, to the $CuInS_2$/carbon electrode with weight ratio of 1:1, the lowest R_{ct} value (18.79 Ω·cm^2) can be achieved, which is in agreement with their cell performance. However, this R_{ct} value is higher than the screen-printed Cu_2S electrode (2.84 Ω·cm^2) in the same symmetric thin layer cell except for using 2 M polysulfide electrolyte (2 M Na_2S and 2 M S).[27]

In our work, no obvious response toward the Warburg impedance of the redox species from the electrolyte is found, which can be regarded as the short circuit. This phenomenon is in agreement with the previous work.[51,52]

The stability of the counter electrode is important to the cell performance of the SSCs. Here, the CdS/CdSe SSCs with $CuInS_2$/carbon electrode were sealed according to our previous work.[27] A preliminary stability test on the CdS/CdSe SSCs with $CuInS_2$/carbon composite electrode has been carried out, which were stored in the dark at room temperature without any

bias voltage or current flow and tested every 2 or 3 days. For comparison, the stability of CdS/CdSe SSCs with carbon electrode was also investigated. Figure 7 gives the variation of

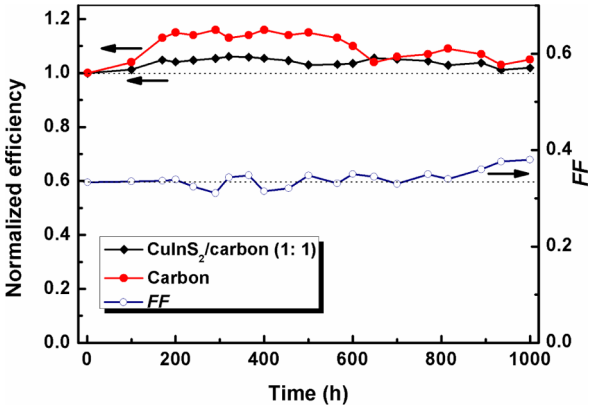

Figure 7. Normalized efficiencies (−♦−) and FF (fill factors, −○−) of the CdS/CdSe SSCs fabricated with $CuInS_2$/carbon composite electrode (weight ratio 1:1) versus conservation time; normalized efficiencies of the CdS/CdSe SSCs with carbon electrode (−●−) versus conservation time.

their normalized efficiencies with 1000 h of conservation time. No obvious degradation of the efficiency for the two SSCs with $CuInS_2$/carbon composite electrode and carbon electrode was found over this period. After 1000 h, for the CdS/CdSe SSCs with $CuInS_2$/carbon composite electrode, the voltage (V_{oc}) and FF were increased by 10.8% and 7.7%, respectively. On the other hand, its photocurrent density J_{sc} dropped by 15.1%, compensated with the increase of V_{oc} and FF, resulting in almost keeping its initial efficiency value after 1000 h. The slow increasing tendency of FF over 1000 h can also be seen in Figure 7. It is thus deduced that the primary stability of the $CuInS_2$/carbon composite electrode with 1 M polysulfide electrolyte is good.

4. CONCLUSIONS

In summary, a ternary chalcopyrite compound $CuInS_2$ has been employed as counter electrode (CE) material for CdS/CdSe cosensitized solar cells (SSCs) for the first time. The CdS/CdSe SSCs with the $CuInS_2$ counter electrode can present 3.63% efficiency under Am 1.5 illumination of 100 mW·cm^{-2}. Furthermore, an appropriate amount of active carbon/carbon black mixture was introduced to reduce the aggregation of the $CuInS_2$ NPs and further increase the electrocatalytic activity and stability; up to 4.32% efficiency has been achieved on the basis of $CuInS_2$/carbon composite electrode with 1:1 weight ratio. With the aid of the electrochemical impedance spectroscopy and *I*−*E* measurement, the electron transfer processes at the interface of $CuInS_2$-based electrodes and polysulfide electrolyte have been investigated in detail. A preliminary long-term stability test of the CdS/CdSe SSCs reveals that the $CuInS_2$/carbon composite counter electrode exhibits good stability after being kept at room temperature for 1000 h. We believe that this $CuInS_2$/carbon composite electrode exhibits good potential application for further investigation.

■ ASSOCIATED CONTENT

Supporting Information

Preparation, *I*−*E*, and stability measurements of the Cu_2S/carbon electrode. Figure S1, comparison of *I*−*E* curves of $CuInS_2$/carbon and Cu_2S/carbon composite electrodes in a three-electrode testing system. Figure S2, the variation of *I*−*E* curves with the conservation time for Cu_2S/carbon composite electrodes based on sealed symmetric thin-layer cells. This information is available free of charge via the Internet at http://pubs.acs.org.

■ AUTHOR INFORMATION

Corresponding Author

*Tel./Fax: +86-10-8264-9242 (Q.M.); +86-10-8264-9005 (D.L.). E-mail: qbmeng@iphy.ac.cn (Q.M.); dmli@iphy.ac.cn (D.L.).

Notes

The authors declare no competing financial interest.

■ ACKNOWLEDGMENTS

The authors appreciate the financial support from the Natural Science Foundation of China (Nos. 20725311 and 51072221) and the Ministry of Science and Technology of China (973 Project, Nos. 2012CB932903 and 2012CB932904). The authors gratefully thank Dr. Zengxia Mei and Mr. Lishu Liu for the resistivity measurement and fruitful discussion.

■ REFERENCES

(1) Nozik, A. J. *J. Physica E* **2002**, *14*, 115−120.
(2) Beard, M. C. *J. Phys. Chem. Lett.* **2011**, *2*, 1282−1288.
(3) Murray, C. B.; Norris, D. J.; Bawendi, M. G. *J. Am. Chem. Soc.* **1993**, *115*, 8706−8715.
(4) Sarma, D. D.; Nag, A.; Santra, P. K.; Kumar, A.; Sapra, S.; Mahadevan, P. *J. Phys. Chem. Lett.* **2010**, *1*, 2149−2153.
(5) Yu, W. W.; Qu, L. H.; Guo, W. Z.; Peng, X. G. *Chem. Mater.* **2004**, *16*, 560−560.
(6) Hotchandani, S.; Kamat, P. V. *J. Phys. Chem.* **1992**, *96*, 6834−6839.
(7) Robel, I.; Subramanian, V.; Kuno, M.; Kamat, P. V. *J. Am. Chem. Soc.* **2006**, *128*, 2385−2393.
(8) Giménez, S.; Mora-Seró, I.; Macor, L.; Guijarro, N.; Lana-Villarreal, T.; Gómez, R.; Diguna, L. J.; Shen, Q.; Toyoda, T.; Bisquert, J. *Nanotechnology* **2009**, *20*, 295204.
(9) Hu, X.; Zhang, Q.; Huang, X.; Li, D.; Luo, Y.; Meng, Q. *J. Mater. Chem.* **2011**, *21*, 15903−15905.
(10) Im, S.-H.; Lim, C.-S.; Chang, J. A.; Lee, Y. H.; Maiti, N.; Kim, H.-J.; Nazeeruddin, M. K.; Grätzel, M.; Seok, S. I. *Nano Lett.* **2011**, *11*, 4789−4793.
(11) Zaban, A.; Micic, O. I.; Gregg, B. A.; Nozik, A. J. *Langmuir* **1998**, *14*, 3153−3156.
(12) Bang, J. H.; Kamat, P. V. *ACS Nano* **2009**, *3*, 1467−1476.
(13) Zhou, N.; Chen, G.; Zhang, X.; Cheng, L.; Luo, Y.; Li, D.; Meng, Q. *Electrochem. Commun.* **2012**, *20*, 97−100.
(14) Zhang, Q.; Guo, X.; Huang, X.; Huang, S.; Li, D.; Luo, Y.; Shen, Q.; Toyoda, T.; Meng, Q. *Phys. Chem. Chem. Phys.* **2011**, *13*, 4659−4667.
(15) Santra, P. K.; Kamat, P. V. *J. Am. Chem. Soc.* **2012**, *134*, 2508−2511.
(16) Hossain, M. A.; Jennings, J. R.; Koh, Z. Y.; Wang, Q. *ACS Nano* **2011**, *5*, 3172−3181.
(17) Grätzel, M.; Janssen, R. A. J.; Mitzi, D. B.; Sargent, E. H. *Nature* **2012**, *488*, 304−312.
(18) Kamat, P. V.; Tvrdy, K.; Baker, D. R.; Radich, J. G. *Chem. Rev.* **2010**, *110*, 6664−6688.

(19) Mora-Seró, I.; Giménez, S.; Fabregat-Santiago, F.; Gómez, R.; Shen, Q.; Toyoda, T.; Bisquert, J. *Acc. Chem. Res.* **2009**, *42*, 1848−1857.
(20) Kay, A.; Grätzel, M. *Sol. Energy Mater. Sol. Cells* **1996**, *44*, 99−100.
(21) Radich, J. G.; Dwyer, R.; Kamat, P. V. *J. Phys. Chem. Lett.* **2011**, *2*, 2453−2460.
(22) Hodes, G.; Manassen, J.; Cahen, D. *J. Appl. Electrochem.* **1977**, *7*, 181−182.
(23) Yang, Z.; Chen, C.-Y.; Liu, C.-W.; Li, C.-L.; Chang, H.-T. *Adv. Energy Mater.* **2011**, *1*, 259−264.
(24) Tachan, Z.; Shalom, M.; Hod, I.; Ruehle, S.; Tirosh, S.; Zaban, A. *J. Phys. Chem. C* **2011**, *115*, 6162−6166.
(25) Hodes, G.; Manassen, J.; Cahen, D. *J. Electrochem. Soc.* **1980**, *127*, 544−549.
(26) Zhang, Q.; Zhang, Y.; Huang, S.; Huang, X.; Luo, Y.; Meng, Q.; Li, D. *Electrochem. Commun.* **2010**, *12*, 327−330.
(27) Fang, B.; Kim, M.; Fan, S.-Q.; Kim, J. H.; Wilkinson, D. P.; Ko, J.; Yu, J.-S. *J. Mater. Chem.* **2011**, *21*, 8742−8748.
(28) Yang, Y.; Zhu, L.; Sun, H.; Huang, X.; Luo, Y.; Li, D.; Meng, Q. *ACS Appl. Mater. Interfaces* **2012**, *11*, 6162−6168.
(29) Meese, J. M.; Manthuruthil, J. C.; Locker, D. R. *Bull. Am. Phys. Soc.* **1975**, *20*, 696−697.
(30) Guha, P.; Gorai, S.; Ganguli, D.; Chaudhuri, S. *Mater. Lett.* **2003**, *57*, 1786−1791.
(31) Cahen, D.; Dagan, G.; Mirovsky, Y.; Hodes, G.; Giriat, W.; Lubke, M. *J. Electrochem. Soc.* **1985**, *132*, 1062−1070.
(32) Mirovsky, Y.; Tenne, R.; Cahen, D.; Sawatzky, G.; Polak, M. *J. Electrochem. Soc.* **1985**, *132*, 1070−1076.
(33) Li, K.; Luo, Y.; Yu, Z.; Deng, M.; Li, D.; Meng, Q. *Electrochem. Commun.* **2009**, *11*, 1346−1349.
(34) Niitsoo, O.; Sarkar, S. K.; Pejoux, C.; Rühle, S.; Cahen, D.; Hodes, G. *J. Photochem. Photobiol., A: Chem.* **2006**, *181*, 306−313.
(35) Imoto, K.; Takahashi, K.; Yamaguchi, T.; Komura, T.; Nakamura, J.; Murata, K. *Electrochem. Commun.* **2003**, *79*, 459−469.
(36) Deng, M.; Huang, S.; Zhang, Q.; Li, D.; Luo, Y.; Shen, Q.; Toyoda, T.; Meng, Q. *Chem. Lett.* **2010**, *39*, 1168−1170.
(37) Ito, S.; Murakami, T. N.; Comte, P.; Liska, P.; Grätzel, C.; Nazeeruddin, M. K.; Grätzel, M. *Thin Solid Film* **2008**, *516*, 4613−4619.
(38) Guo, X.-Z.; Luo, Y.-H.; Zhang, Y.-D.; Huang, X.-M; Li, D.-M.; Meng, Q.-B. *Rev. Sci. Instrum.* **2010**, *81*, 103106.
(39) Guo, X.-Z.; Luo, Y.-H.; Li, C.-H.; Qin, D.; Li, D.-M.; Meng, Q.-B. *Curr. Appl. Phys.* **2012**, *12*, e54−e58.
(40) Deng, M.; Zhang, Q.; Huang, S.; Li, D.; Luo, Y.; Shen, Q.; Toyoda, T.; Meng, Q. *Nanoscale Res. Lett.* **2010**, *5*, 986−990.
(41) Sing, K. S. W.; Everett, D. H.; Haul, R. A. W.; Moscou, L.; Pierotti, R. A.; Rouquérol, J.; Siemieniewska, T. *Pure Appl. Chem.* **1985**, *57*, 603−619.
(42) Sun, H.; Qin, D.; Huang, S.; Guo, X.; Li, D.; Luo, Y.; Meng, Q. *Energy Environ. Sci.* **2011**, *4*, 2630−2637.
(43) Hao, F.; Dong, P.; Zhang, J.; Zhang, Y.; Loya, P. E.; Hauge, R. H.; Li, J.; Lou, J.; Lin, H. *Sci. Rep.* **2012**, *2*, 368.
(44) Wu, M.; Lin, X.; Hagfeldt, A.; Ma, T. *Angew. Chem., Int. Ed.* **2011**, *50*, 3520−3524.
(45) Zhang, Z.; Zhang, X.; Xu, H.; Liu, Z.; Pang, S.; Zhou, X.; Dong, S.; Chen, X.; Cui, G. *ACS Appl. Mater. Interfaces* **2012**, *4*, 6242−6246.
(46) Papageorgiou, N. *Coord. Chem. Rev.* **2004**, *248*, 1421−1446.
(47) Hauch, A.; Georg, A. *Electrochim. Acta* **2001**, *46*, 3457−3466.
(48) Murakami, T. N.; Ito, S.; Wang, Q.; Nazeeruddin, M. K.; Bessho, T.; Cesar, I.; Liska, P.; Humphry-Baker, R.; Comte, P.; Péchy, P.; Grätzel, M. *J. Electrochem. Soc.* **2006**, *153*, A2255−A2261.
(49) Bisquert, J. *J. Phys. Chem. B* **2002**, *106*, 325−333.
(50) Bisquert, J.; Mora-Seró, I. *J. Phys. Chem. Lett.* **2010**, *1*, 450−456.
(51) González-Pedro, V.; Xu, X.; Mora-Seró, I.; Bisquert, J. *ACS Nano* **2010**, *4*, 5783−5790.
(52) Zhang, Q.; Chen, G.; Yang, Y.; Shen, X.; Zhang, Y.; Li, C.; Yu, R.; Luo, Y.; Li, D.; Meng, Q. *Phys. Chem. Chem. Phys.* **2012**, *14*, 6479−6486.